

# Quantum Chaos of a particle in a square well : Competing Length Scales and Dynamical Localization

R. Sankaranarayanan\*, A. Lakshminarayan† and V. B. Sheorey‡

*Physical Research Laboratory,  
Navrangpura, Ahmedabad 380 009, India.*

## Abstract

The classical and quantum dynamics of a particle trapped in a one-dimensional infinite square well with a time periodic pulsed field is investigated. This is a two-parameter non-KAM generalization of the kicked rotor, which can be seen as the standard map of particles subjected to both smooth and hard potentials. The virtue of the generalization lies in the introduction of an extra parameter  $R$  which is the ratio of two length scales, namely the well width and the field wavelength. If  $R$  is a non-integer the dynamics is discontinuous and non-KAM. We have explored the role of  $R$  in controlling the localization properties of the eigenstates. In particular the connection between classical diffusion and localization is found to generalize reasonably well. In unbounded chaotic systems such as these, while the nearest neighbour spacing distribution of the eigenvalues is less sensitive to the nature of the classical dynamics, the distribution of participation ratios of the eigenstates proves to be a sensitive measure; in the chaotic regimes the latter being lognormal. We find that the tails of the well converged localized states are exponentially localized despite the discontinuous dynamics while the bulk part shows fluctuations that tend to be closer to Random Matrix Theory predictions. Time evolving states show considerable  $R$  dependence and tuning  $R$  to enhance classical diffusion can lead to significantly larger quantum diffusion for the same field strengths, an effect that is potentially observable in present day experiments.

PACS numbers: 05.45.M, 72.15.R, 68.65.F

---

\*sankar@prl.ernet.in

†arul@prl.ernet.in

‡sheorey@prl.ernet.in

## I. INTRODUCTION

For several years now studies on quantized chaotic systems have increased significantly with the object of revealing quantum mechanical manifestations of classical chaos [1,2]. The bulk of the work has used smooth Hamiltonian systems. If we start perturbing an integrable system, classical Hamiltonian chaos may develop through a gradual destruction of invariants. The celebrated Kolmogorov-Arnold-Moser (KAM) theorem gives conditions as to when a given tori would be only distorted. This scenario has been widely studied in two degree of freedom systems or two-dimensional area preserving maps. However, there are conditions upon which the KAM theorem rests that may not always be satisfied by certain systems of physical interest. In particular if the perturbation is not sufficiently smooth or even discontinuous the KAM scenario may break down. Large scale chaos may instantaneously develop in the system. One other way is that the KAM scenario fails when the unperturbed system is fully resonant, as in the Kepler problem. We deal in this paper with the former kind of non-KAM behaviour.

We first discuss the prevalence of systems where such effects may be seen. The simplest systems where Hamiltonian chaos can develop is the so called 1.5 degree of freedom system, which are time-dependent one-degree of freedom systems. Thus consider the rotor Hamiltonian:

$$H = \frac{p_\theta^2}{2} + f(t)V(\theta)$$

where  $V(\theta)$  is an external potential that is periodic with period  $2\pi$ , and  $f(t)$  is a periodic function of time with period  $T$ . A lengthening pendulum for instance may be the system under study. If  $V(\theta)$  is sufficiently smooth, the KAM theorem scenario combined with the Poincare-Birkhoff theorem provides the generic behaviour. The smoothness or at least continuity of  $V(\theta)$  is provided by the periodic boundary conditions in angular position of the rotor. Introducing discontinuous potentials will lead to delta function forces equivalent to walls of certain heights.

This brings us to a natural class of systems where non-KAM behaviour will be the rule rather than the exception: externally forced particles in wells. This forms a broad class of systems which have evoked considerable interest and research since the development of quantum wells and dots. One of the experiments where quantum “scarring” of wave functions was reported involved resonant tunneling of a particle across a well in which there were external electromagnetic fields [3].

In fact the simplest of such systems involve a particle in one-dimensional infinite square wells (1-d billiards) with time-dependent external fields. Consider as an example the Hamiltonian:

$$H = H_0 + \epsilon \cos(\omega t) \cos(2\pi x/\lambda) \tag{1}$$

where  $H_0 = p^2/2 + V_{sq}(x; a)$ , describing such a particle. The potential  $V_{sq}(x; a)$  is the confining infinite square well potential of width  $2a$ , centered at the origin. Here  $\epsilon$  and  $\lambda$  are field strength and wavelength of the external field which is being modulated in time with frequency  $\omega$ .

It is easy to verify that the equations of motion are invariant under the following transformation:

$$t \rightarrow \omega_0 t, \quad p \rightarrow p/2a\omega_0, \quad x \rightarrow x/2a,$$

and

$$\epsilon \rightarrow \epsilon/(2a\omega_0)^2, \quad \lambda \rightarrow \lambda/2a, \quad \omega \rightarrow \omega/\omega_0.$$

Here the frequency  $\omega_0$ , which sets the new time scale, is arbitrary. Note that the new scaled variables and parameters are referred by the old symbols and they are dimensionless. Setting  $\omega_0 = \omega$  in the above transformation, we have effectively two parameters :  $\epsilon$  and  $R = 2a/\lambda$ . Here  $R$  is the ratio of two length scales of the system i.e., well width and field wavelength. The presence of two competing length scales, provides a rich range of non-KAM behaviours. In particular if the dimensionless ratio  $R$  is a non-integer there is a possibility of observing non-KAM phenomena.

Under the perturbation we can expect roughly that states whose absolute value of the initial momentum is less than  $\sqrt{2|\epsilon|}$  will be most affected. Thus low energy states will be most affected by the time-dependent forces. Fig. 1 shows the effect of the parameter  $R$ . While for  $R = 1$  the system is essentially KAM and has KAM tori interspersed with resonances, any small deviation of  $R$  away from unity destroys low energy KAM curves and leads to increased chaos. Fig. 2 shows the fate of an individual KAM torus for which  $R = 1$  is a “bifurcation” point in parameter space and changes stability on either side. We expect such behaviour to be generic to a large class of similar systems and in this paper we will exhaustively study a “standard map” version of these systems. Just as the standard map provides an abstracted view of behaviour around nonlinear resonances we expect our model’s analysis to provide such a view for these systems.

Many models have been studied where the time dependence  $f(t)$  is a train of Dirac delta functions, the periodically kicked systems [4]. The reasons are evident: they are the simplest Hamiltonian systems where many generic features of chaotic complex systems may be observed; and they allow a partial integration of the equations of motion, from kick to kick, enabling us to study iterative “mappings” rather than differential equations. Quantum mechanically the simplification enables us to partially integrate the Schrödinger equation and write the kick to kick propagator, or Floquet operator, analytically [5].

An important paradigm in this class is the delta kicked rotor from which is derived the standard map [6,7]. The dynamical richness of the classical system which obeys the KAM theorem and the consequent smooth transition to chaos is now well known, and fairly understood [8–10]. The corresponding quantum system has also been studied quite extensively as a model of “quantum chaos” (see [11] for an early review on this), and continues to provide an excellent model to numerically test our understanding of such systems [12].

The periodic input of energy into the system through the kicks can result in a diffusive increase of the momentum, and strong kicking strength can lead to unbounded energy growth classically. However, an important result on quantization is that the eigenfunctions (quasienergy states) are generically *exponentially localized in momentum space*, which suppresses the momentum diffusion even in the highly chaotic regime. A plausible mechanism for this “dynamical localization” was suggested when an analogy was found [13] to Anderson

type localization of electrons in random on-site potentials [14]. Experimental realizations of the delta kicked rotor, with cold atoms in pulsed standing laser fields [15], has confirmed the quantum suppression of diffusion. The localized states in unbounded momentum space results in quasi-independence of the quasienergies, and the random matrix properties [16,1] expected of quantized chaotic systems are not seen. For instance the nearest neighbour spacing distribution is Poisson rather than Wigner and the eigenfunction components are not gaussian distributed. It must be stated that most of these results are numerical and larger matrix calculations that are “more semiclassical” may show spectral transitions as the bulk of the eigenfunctions spread out and overlap with each other while the tails are still exponentially localized. Some evidence of this will also be present in this paper.

Following our motivational discussion above, we replace the time dependence by a series of delta functions to facilitate the derivation of a map in which we can study non-KAM behaviour of the kind suggested above. Recently study of such systems has begun [17,18]. For instance in [17] it is shown that the quantum states are extended and delocalized in the highly chaotic (strong field) regime. In turn, the spacing distribution of the quasienergies, unlike the kicked rotor, follow the Wigner distribution. It is argued that the extended states do overlap and hence the corresponding quasienergies are not independent, resulting in level repulsion. Part of the present paper also critically examines these results. In [18] a classical analysis of a generalized system has been carried out to understand the changes of stability that occur as a function of  $R$  and some of these results will be summarized below.

## II. CLASSICAL SYSTEM

The system of interest is a particle inside the potential  $V_{sq}(x; a)$  in the presence of a particular time-periodic impulse. We consider the Hamiltonian given by

$$H = H_0 + \epsilon \cos(2\pi x/\lambda) \sum_{n=-\infty}^{\infty} \delta(n - t/T). \quad (2)$$

Kick-to-kick dynamics of the particle immediately after each pulse can be described by an area preserving map which in dimensionless form is

$$\begin{aligned} X_{n+1} &= (-1)^{B_n} \{(X_n + P_n) - \text{Sgn}(P_n)B_n\} \\ P_{n+1} &= (-1)^{B_n} P_n + (K/2\pi) \sin(2\pi R X_{n+1}). \end{aligned} \quad (3)$$

Here  $B_n = [\text{Sgn}(P_n)(X_n + P_n) + 1/2]$  is the number of bounces of the particle between the walls during the interval between  $n$ th and  $(n + 1)$ th kick, [...] stands for the integer part of the argument. The state of the particle just after the  $n$ th kick is now given in the new variables as  $X_n, P_n$ . The sign of the momentum ( $\pm 1$ ) is given by  $\text{Sgn}(P_n)$ . The following scaling relations are used to redefine the variables and parameters:

$$X_n = \frac{x_n}{2a}, \quad P_n = \frac{p_n T}{2a}, \quad K = \frac{2\epsilon\pi^2 T^2}{a\lambda}, \quad R = \frac{2a}{\lambda}. \quad (4)$$

We note that  $|X_n| \leq 1/2$  and effective parameters of the particle dynamics are  $K$ , the field strength and  $R$ , the ratio of the two length scales. The map in (3) shows the principal

features that we have discussed earlier in the introduction and may qualify as a “standard” map for such non-KAM systems. In fact there is a close relationship between this “well-map” (3) and the standard map itself that allows us to study it as a *Generalized Standard Map* (GSM) [18]. This is the map:

$$\begin{aligned} P_{n+1} &= P_n + (K/2\pi) \sin(2\pi R X_n) \\ X_{n+1} &= X_n + P_{n+1} \pmod{1} \end{aligned} \tag{5}$$

which is defined on a cylinder  $(-\infty, \infty) \times [-1/2, 1/2)$ . The well-map and the GSM differ only by boundary conditions i.e., the former and latter have reflective and periodic boundary conditions respectively. It is easy to see that this does not play any effective role, in the sense that the trajectories as evolved under the two systems can at most differ by a sign, depending on the number of bounces undergone. This fact simplifies considerably our analysis of the well-map. When  $R = 1$ , the GSM is the well studied and fairly understood standard map of the delta-kicked rotor.

Dynamics of the GSM is highly chaotic and diffusive in the strong field regime ( $K \gg 1$ ). In addition, it exhibits other interesting features like the development of chaos and hence diffusion even in the weak field regime ( $K < 1$ ) when  $R \neq j$  where  $j$  is a positive integer, see Fig. 3. Note that the phase space portrait of both the well-map and the GSM are same. Such dynamical features are in fact common in non-KAM systems and one such situation is shown earlier. We can understand the development of chaos at low field strengths from the observation that the otherwise continuous map is discontinuous when  $R \neq j$ . The KAM theorem does not hold for the discontinuous case and no smooth KAM tori exist in the phase space, however small  $K$  may be. In the absence of KAM tori, the phase space is chaotic and diffusive even in the weak field regime. More over, when  $R < 1/2$  the GSM is a hyperbolic system. For a more detailed investigation of the GSM we refer the reader to [18].

### III. QUANTUM MECHANICS OF THE TRAPPED PARTICLE

For the Hamiltonian which is periodic in time with period  $T(= 2\pi/\omega)$ , solutions of the Schrödinger equation satisfy the eigenvalue equation [19]

$$U|\psi_j\rangle = e^{-i\alpha_j T/\hbar}|\psi_j\rangle \tag{6}$$

where  $U$  is the one period time evolution operator. Here  $|\psi_j\rangle$  and  $\alpha_j$  are the quasienergy states and quasienergies respectively. It is to be noted that the inner product of two arbitrary solutions of the Schrödinger equation for arbitrary time dependent Hamiltonian is independent of time due to hermiticity of the Hamiltonian. As a consequence of this, states correspond to  $\alpha_i$  and  $\alpha_j$  such that  $\alpha_i - \alpha_j \neq n\hbar\omega$  (where  $n$  is an integer) are orthogonal at a given time. If  $\alpha_i - \alpha_j = n\hbar\omega$ , the states are degenerate and hence the quasienergies are uniquely defined with modulo  $\hbar\omega$ . From the set of all orthogonal states we may write the general solution at a given time as  $|\Psi\rangle = \sum_j c_j |\psi_j\rangle$ .

## A. Matrix Representation of $U$

Periodically kicked systems are particularly easy to study since  $U$  can be written immediately by integrating the Schrödinger equation between successive kicks. For the Hamiltonian  $H$  in Eq. (2) we have

$$U = \exp \left\{ -ik \cos \left( \frac{2\pi x}{\lambda} \right) \right\} \exp \left\{ -i \frac{H_0 T}{\hbar} \right\} \quad (7)$$

where  $k = \epsilon T / \hbar$ . Note that the above time evolution operator is the quantum counter part of the well-map and not that of the GSM. The eigensystem in Eq. (6) may be solved by diagonalizing a matrix representation of  $U$ . The natural choice of basis for the  $U$ -matrix is the eigenstates of the unperturbed Hamiltonian  $H_0$ :

$$H_0 |n\rangle = E_n |n\rangle \quad (8)$$

where  $n = 1, 2, 3, \dots$ . The energy eigenfunctions and eigenvalues are

$$\langle x | n \rangle = \begin{cases} \frac{1}{\sqrt{a}} \cos\left(\frac{n\pi x}{2a}\right), & \text{for } n \text{ odd} \\ \frac{1}{\sqrt{a}} \sin\left(\frac{n\pi x}{2a}\right), & \text{for } n \text{ even} \end{cases} ; \quad E_n = \frac{n^2 \pi^2 \hbar^2}{8a^2}. \quad (9)$$

The unitary matrix  $U$  is then calculated as:

$$U_{mn} = \langle m | U | n \rangle = \langle m | \exp\{-ik \cos(2\pi x/\lambda)\} | n \rangle e^{-in^2\tau} \equiv F_{mn} e^{-in^2\tau} \quad (10)$$

where we have defined an effective Planck constant as

$$\tau = \frac{\pi^2 \hbar T}{8a^2}. \quad (11)$$

As the external field preserves parity we have

$$F_{mn} = \begin{cases} 0, & \text{if } m+n \text{ is odd} \\ \frac{1}{2\pi} \left\{ Q_{\frac{m-n}{2}} - (-1)^n Q_{\frac{m+n}{2}} \right\}, & \text{if } m+n \text{ is even} \end{cases} \quad (12)$$

where

$$Q_l = \int_{-\pi}^{\pi} \cos(l\theta) e^{-ik \cos(R\theta)} d\theta \quad (13)$$

and  $\theta = \pi x/a$ . We note that  $Q_l$  is a Bessel function integral for integer  $R$ , while for non-integer  $R$  the integral constitutes a kind of ‘‘incomplete’’ Bessel function. Invoking the Bessel function  $J_s(k)$  through the following identity

$$e^{-ik \cos \theta} = \sum_{s=-\infty}^{\infty} (-i)^s J_s(k) e^{-is\theta}$$

the integral can be evaluated as a series:

$$Q_l = 2\pi J_0(k) \delta_{l,0} + 2 \sum_{s=1}^{\infty} (-i)^s J_s(k) C_s \quad (14)$$

where

$$C_s = \int_{-\pi}^{\pi} \cos(l\theta) \cos(sR\theta) d\theta = \begin{cases} \frac{(-1)^l 2sR \sin(sR\pi)}{(sR)^2 - l^2}, & \text{for } sR \neq |l| \\ \pi, & \text{for } sR = |l| \end{cases}.$$

The relation  $J_{-s}(k) = (-1)^s J_s(k)$  has been used in Eq.(14). Note that if  $R$  is an integer, Eq.(14) simplifies to

$$Q_l = 2\pi \sum_{s=0}^{\infty} (-i)^s J_s(k) \delta_{|l|,sR} \quad (15)$$

and a single term is picked out of the infinite series.

The forms of  $Q_l$  allow us to assess the fall of the matrix elements of the unitary matrix  $U$ . For integer  $R$  the unitary matrix can be essentially banded as the matrix elements fall off exponentially after a certain cut-off. For  $R = 1$ , as is well known and can be seen from above for  $l > k$  the matrix elements fall off exponentially, where  $l$  measures the distance from the diagonal. On the other hand when  $R$  is not an integer, apart from the Bessel function terms there are terms that are falling only polynomially in  $l$ . For instance when  $R = 1/2$  we have

$$Q_l = 2\pi(-1)^l J_{2l}(k) + (-1)^l 8 \sum_{s=1,3,5,\dots}^{\infty} \frac{(-i)^s s \sin(s\pi/2)}{s^2 - 4l^2} J_s(k). \quad (16)$$

The infinite series gets effectively cut-off for  $s > k$ . The finite sum has terms that only decay as  $l^{-2}$ . Thus non-integer  $R$  values imply an important characteristic of the unitary quantum map: the polynomial fall of matrix elements, as opposed to the exponential fall characterizing integer  $R$ . In fact we may speculate whether non-KAM systems are *always* characterized by polynomially decaying matrix elements in the unperturbed basis. According to earlier studies eigenfunction localization crucially depends on the way in which matrix elements fall.

When  $R = 1$ , the classical equivalence of the kicked rotor to the particle in a well was noted above. It is easy to see that quantum mechanically also the equivalence persists. The parity symmetry reduced rotor unitary matrix is identical to the well unitary operator in this case and hence odd states of the rotor correspond to the odd states of well, while the even states have a similar relationship. Thus all that is known for the quantum standard map, including exponential localization of eigenstates, may be carried over to the well system with  $R = 1$ . This allows us to address interesting questions of deviations from the standard map in a single model.

The perturbing potential  $\cos(2\pi x/\lambda)$  preserves the parity of  $H_0$ , and hence  $U$  has the symmetry of parity. In what follows we consider only the states which have odd parity. In addition, the system has a spatial translational symmetry when  $R$  is an integer. Let us define a transformation for integer  $R$  as

$$\mathcal{T}f(X) = f((X + 1/R) \bmod 1) \quad (17)$$

such that  $\mathcal{T}^R f(X) = f(X)$ .  $\mathcal{T}$  has the eigenvalues  $\beta_l = \exp(i\frac{2l\pi}{R})$  where  $l = 0, 1, 2, \dots, (R-1)$ . The commutation relation  $[U, \mathcal{T}] = 0$  leading to  $\mathcal{T}|\psi\rangle = \beta_l|\psi\rangle$ . For  $R = 2$ ,  $\beta_l = \pm 1$ ; in this case we consider only the states which correspond to  $\beta_l = 1$ .

Dimensionless quantum parameters  $k$  and  $\tau$  are related to the classical parameters through the relation  $K/R = 8k\tau$ . The semiclassical limit is  $k \rightarrow \infty$  and  $\tau \rightarrow 0$ , such that  $k\tau$  is fixed. Any arbitrary state of the system at a given time is  $|\Psi(t)\rangle = \sum_n A_n(t)|n\rangle$  and its time evolution is given by  $A_m(t+T) = \sum_n U_{mn}A_n(t)$ .

## B. Quantum Resonance

Here we investigate if the parameter  $R$  has any effect on the important phenomenon of “quantum resonance”. We notice that the unperturbed motion of the particle, given by the Hamiltonian  $H_0$ , between the kicks simply adds phase to the wave function components (when expressed in the unperturbed basis, as in Eq. (10)). At resonance ( $\tau = 2\pi$ ), the unperturbed motion between the kicks is absent. In this case, without loss of generality, the time evolution of an arbitrary state of the system is

$$|\Psi(t)\rangle = e^{-ik \cos(2\pi x/\lambda)t} |\Psi(0)\rangle \quad (18)$$

and thus  $|\Psi(t)|^2 = |\Psi(0)|^2$ . Note that here  $t$  is the number of kicks. The kinetic energy of the particle is then

$$E(t) = E(0) + \frac{-\hbar^2}{2} \left\{ \left( \frac{4\pi kt}{\lambda} \right) \int_{-a}^a \sin\left(\frac{2\pi x}{\lambda}\right) \operatorname{Re} \left\{ i\Psi^*(0) \frac{\partial \Psi(0)}{\partial x} \right\} dx - \left( \frac{2\pi kt}{\lambda} \right)^2 \int_{-a}^a |\Psi(0)|^2 \sin^2\left(\frac{2\pi x}{\lambda}\right) dx \right\}. \quad (19)$$

In the limit  $t \rightarrow \infty$  energy grows quadratically with the number of kicks. If  $|\Psi(0)\rangle = |n\rangle$ , i.e., the initial state is one of the unperturbed state itself, the energy is purely quadratic. In fact, the energy can be found exactly as

$$E(t) = E(0) \left\{ 1 + \left( \frac{ktR}{n} \right)^2 (2 - A) \right\} \quad (20)$$

where

$$A = \begin{cases} \frac{\sin(2\pi R)}{\pi R} \left( \frac{n^2}{n^2 - 4R^2} \right) & \text{if } n \neq 2R \\ (-1)^{n+1} & \text{if } n = 2R \end{cases}.$$

Since  $A \neq 2$ , we observe that the quadratic energy growth is unaffected by the length scale ratio  $R$ . Numerically we have found that this behaviour is seen when  $\tau$  is rational multiples of  $2\pi$  also. Thus the quantum resonance phenomena of the well system is very similar to that of the kicked rotor [6,20]. It is to be noted that resonance is a non-generic pure quantum phenomena and no correspondence to it can be seen in the classical system. In the context of a particle in a well, quantum resonance may lead to enhanced ionization in a finite well.



## IV. RESULTS

Having given sufficient description of the system under investigation, here we analyze quasienergy states and quasienergies of the generic quantum system ( $\tau$  is irrational multiples of  $2\pi$ ) in relevant classical regimes. On taking a truncated  $N$  dimensional Hilbert space spanned by the first  $N$  unperturbed basis states which belong to odd parity, diagonalization of the matrix  $U_{mn}$  gives the eigenstates  $\{|\psi\rangle\}$  such that  $|\psi\rangle = \sum_n \psi_n |n\rangle$ . We consider only states that are “converged” in the sense that they are independent of the truncation size  $N$ . Thus the states we are interested in belong to that of the infinite Hilbert space; they are states of the infinite cylinder and *not* of a truncated cylinder, or torus. The last distinction becomes important as quantum states that belong to the cylinder can have completely different localization features than those that belong to a truncated cylinder. As we are interested in a particle in an infinite potential well, such a truncation lacks physical meaning.

### A. Localization measures of eigenstates

Localization can be measured using a unified quantity, the Renyi Participation Ratio  $\xi_q$

$$\xi_q = \left( \sum_n |\psi_n|^{2q} \right)^{1/(q-1)} \quad (21)$$

of which the entropy and participation ratio (PR) are special cases. In our analysis we first use a normalized information entropy as a measure of localization of states, and this is defined as:

$$S = \frac{-1}{\ln(N/2)} \sum_{n=1}^N |\psi_n|^2 \ln |\psi_n|^2. \quad (22)$$

It is easy to see that  $S = \ln \xi_1 / \ln(N/2)$ . This measure compares the entropy to that of the eigenfunctions of  $N \times N$  matrices belonging to the Gaussian Orthogonal Ensemble (GOE) which is approximately  $\ln(N/2)$ . The GOE is relevant to time reversal symmetric systems such as we are considering.

First we calculate a gross measure of localization in a given spectrum by averaging over all converged states. We set criteria for the states to be converged so that the states belong to the cylinder, or are at least very close to states that belong to the cylinder. In all the following cases, the eigenvalues are converged in modulus to unity to within 0.0001 or better. Fig. 4 shows the average entropy as a function of  $R$ . For small  $K$  ( $\leq 1$ ), the oscillations are qualitatively similar with distinct entropy minima at integer  $R$  and maxima at around half-integer  $R$ . This may provide a simple mechanism to experimentally control the extent of localization. The information entropy is of course basis dependent; the unperturbed basis we use is a useful one as it has information about localization in the momentum.

Naturally, the minima in entropy is expected to have strong associations with the presence of stable regions in the classical phase space. Of special significance are KAM tori in phase space, as these structures are complete barriers to classical diffusion in momentum. In spite of the fact that in the classical system all the KAM tori break up in the standard map

( $R = 1$ ) at  $K = 1$ , we observe a minimum entropy. This is due to the presence of cantori which are partial barriers for chaotic orbits and suppresses global diffusion. For non-integer  $R$  a complex phase space picture emerges and has been discussed in [18]. Maximum entropy around half-integer  $R$  is the classical parametric regime where the discontinuity is maximum corresponding to the maximum chaos assisted diffusion.

For large  $K$  ( $= 10$ ), oscillations in entropy are still present while there is apparently complete chaos for all relevant  $R$  values. We can understand these oscillations as due to the strong correlation between the localization of eigenstates and classical diffusion coefficient. For  $R < 1/2$  the semiclassical parameter  $k = K/(8R\tau)$  is large, yet there is increased localization of states due to limited classical diffusion, presumably due to the presence of cantori. For the kicked rotor the exponential localization length was found to be proportional to the classical diffusion coefficient [21]. This was found by numerical experiments and is supported by certain qualitative arguments. We are now in a position to examine the relationship between quantum localization and classical diffusion in the context of the particle in a well, wherein we have the freedom of another control parameter, namely  $R$ , with which to vary the classical diffusion.

Instead of studying localization lengths we study here the measures of localization such as the entropy or the PR. We study the PR more closely rather than the entropy. In chaotic regimes we have numerically ascertained that exponential of the entropy is proportional to the PR, as shown in Fig. 5. The relationship between the localization length hitherto calculated for the kicked rotor and the PR calculations we present will need more detailed study, but we expect them to be roughly proportional to each other. In fact if we assume a fully exponentially localized state with  $|\psi_n| \sim \exp(-|n - n_0|/l_\infty)$ , then the PR is

$$\xi_2^{-1} = \left( \sum_n |\psi_n|^4 \right)^{-1} = 2l_\infty. \quad (23)$$

We recapitulate the argument connecting classical diffusion and the localization length for the specific system we are considering, as there are difference in factors. On considering time evolution of an initial state, kinetic energy diffuses for a certain time  $t_c$  and then attains quasiperiodic saturation. The number,  $n_c$ , of unperturbed states that are excited during the time evolution is related to the critical time by the diffusion equation:

$$\pi^2 \hbar^2 n_c^2 = D_{\text{CL}} t_c \quad ; \quad \langle (p_t - p_0)^2 \rangle = D_{\text{CL}} t \quad (24)$$

where  $D_{\text{CL}}$  is the classical diffusion coefficient in momentum and  $\langle \dots \rangle$  represents the ensemble average. Here the momenta and the diffusion coefficient have dimensions and we have taken  $a = 1/2$ . The critical time being the Heisenberg time relevant for  $n_c$  equally spaced eigenstates, we get  $t_c \sim n_c T / 2\pi$ . If the average localization length  $\langle l_\infty \rangle$  is also  $n_c$ , we obtain the relation :

$$\langle \xi_2^{-1} \rangle = 2 \langle l_\infty \rangle = \frac{\alpha \pi}{4\tau^2} D(K, R) \quad (25)$$

where  $\tau$  is the dimensionless effective Planck constant defined in Eq. (11) and  $\alpha$  is a constant whose value has been numerically determined as 1/2 for the standard map [22].  $D(K, R)$  is the dimensionless diffusion coefficient which one will get from using the dimensionless maps Eq. (3) or Eq. (5). The dependence on *both*  $K$  and  $R$  is emphasized.

In Fig. 6 we show the average PR and the scaled diffusion coefficient according to the relation Eq.(25). We see that the relation derived above holds in some parameter regions while it picks up only qualitative features of the oscillations in the others. In particular the relation seems to hold for  $R < 1/2$  when the classical system is hyperbolic as well as around  $R = 1$ . The deviations from the relation (25) might be due to fluctuations of the state components in the unperturbed basis (one such case is shown in Fig. 11). These fluctuations may lead to different scaling behaviour between the average PR and the classical diffusion coefficient. However more detailed investigations are needed to make any positive statements. The sharp deviation for  $R = 2$  can be accounted for as due to the presence of an extra quantum symmetry discussed above.

Following our study on average PR and its scaling with the classical diffusion coefficient, we may then enquire about how the PR itself is distributed in a given spectrum if the average reflects the general behaviour. We find that when the classical system is chaotic, the distribution of a normalized quantity  $y = \ln \xi_2^{-1} / \langle \ln \xi_2^{-1} \rangle$  (this is similar to the distribution of the entropy due to the linear relationship exhibited above) is nearly normal as seen in Fig. 7. This may be attributed to a realization of the Central Limit Theorem. However the PRs and Inverse Participation Ratios (IPRs) themselves are not normal. Their distributions may be got by assuming that the distribution of  $y$  is normal. Thus the PRs are distributed according to the lognormal distribution [23]:

$$\Lambda(\xi_2^{-1}) = \frac{1}{\sqrt{2\pi}\sigma\langle\ln\xi_2^{-1}\rangle\xi_2^{-1}} \exp\left\{-\frac{1}{2\sigma^2}\left(\frac{\ln\xi_2^{-1}}{\langle\ln\xi_2^{-1}\rangle}-1\right)^2\right\} \quad (26)$$

where  $\sigma^2$  is the variance of  $y$ . As an immediate consequence, distribution of IPRs is also lognormal. Distribution of such localization measures are much of significance. Recently the distribution of IPRs have been exploited to show that the distribution of resonance widths in wave-chaotic dielectric cavities is lognormal [24].

When  $K$  is small ( $\leq 1$ ), the classical motion is nearly regular for  $R = 1$ , while chaotic for  $R \leq 0.5$ . However the time scales for classical diffusion is large making the observation of  $R$  effects on quantum dynamics hard to discern. For instance the nearest neighbour spacing distribution may remain very close to the Poisson distribution. In such a situation we find that the distribution of the PRs provides a positive litmus test. In Fig. 8 such an example is shown, wherein even for small field strengths the effect of  $R$  is clearly visible as a tendency for  $y$  to be normally distributed. This is an indication of the ‘‘delocalization’’ that is taking place in the eigenfunctions. This delocalization is limited in the sense that while the eigenfunctions remain square integrable there is more spreading out in the bulk part of the states. Thus we may conclude that distribution of the localization measures is a sensitive quantity in chaotic quantum systems.

Time evolution of non-stationary states must reflect the properties of the stationary states and is also of importance in the context of experiments. Here we have studied the diffusion in kinetic energy of a state  $|\Psi\rangle$  which is initially the ground state of the unperturbed system. We illustrate with one example wherein for a fixed classical parameter  $K$ , the effects of non-integer  $R$  is seen clearly for a given  $\tau$  value. Thus tuning  $R$  essentially tunes  $\lambda$  since  $a$  is fixed through the relation (11). In Fig. 9 scaled kinetic energy  $\langle P^2 \rangle = \langle \Psi | P^2 | \Psi \rangle$  is shown as a function of time (number of kicks) for a small value of  $K$  corresponding to a small classical field strength  $\epsilon$ . We note that while the quantum diffusion saturates at a

much higher value for  $R = 1.5$ , compared to  $R = 1$ , the actual classical field strength  $\epsilon$  (from Eq. (4)) is *smaller* by a factor of 1.5. For comparison is shown another integer case,  $R = 2$ , wherein the classical diffusion is smaller compared to  $R = 1$ .

## B. Eigenvalues and Eigenstates

It is clear from our earlier observations that the states are more localized in the regular or mixed regimes of the classical system while less localized (or delocalized) in the chaotic regimes. The degree of localization is also controlled by the ratio of the length scales and complexity of the classical phase space is reflected in the localization measures. Here we look at the quasienergies and the corresponding states more closely.

In Fig. 10 we have shown the nearest neighbour spacing distribution of the quasienergies for various parameters. The first row and the last column of the catalogue correspond to classically chaotic regimes and the rest belong to the regular/mixed phase space regimes. In regular/mixed regimes where the states are highly localized, the spacing shows excellent agreement with the Poisson distribution. On the other hand, in chaotic regimes the spacing agrees well with the Poisson distribution except at small spacings. This is due to the fact that bulk part of the eigenstates are delocalized and they overlap each other. However, the tail part of the states are exponentially localized and the degree of overlap is not significant enough. We also notice that the spacing distribution is only slightly sensitive to the nature of the classical dynamics in the case of the unbounded kicked rotor or the well, at least in the parameter regimes we have investigated. In such situations, as we have demonstrated earlier, the distribution of PRs is a good measure to distinguish the chaotic quantum systems from the regular systems.

Our extensive calculations of the eigenstates in chaotic regimes show that, in general, it is hard to qualitatively differentiate the states corresponding to non-integer  $R$  values from the rotor ( $R = 1$ ) states as far as their localization behaviour is concerned. In particular it is not easy to distinguish the emergence of non-exponential tails unequivocally. However, we found that eigenstates corresponding to non-integer  $R$  values generally have more fluctuations compared to the rotor states; this is illustrated with some examples in Fig. 11. The fluctuations are closer to the RMT predictions in the case of non-integer  $R$  values and is shown further below.

Recently there have been studies on the special case ( $R = 0.5$ ) of the system (2), with the motivation of revealing quantal behaviour of non-KAM systems [17]. It was observed that the quasienergy states are “extended” in the unperturbed basis and as a result the spacing distribution was shown to be Wigner distributed. At this juncture we would like to compare our results with certain aspects of this work. In [17], the eigenstate shown in the highly chaotic regime ( $K = 50, N = 1024$ ; we have not been able to ascertain the value of  $\tau$  used in this work) does *not* appear to belong to the unbounded phase space as it spreads all over the basis. Thus while states such as these may belong to some truncated dynamical system, it does not belong to the infinite Hilbert space of the well system. Increasing the dimensionality of the matrix used will modify such states; in short they are not converged. As we demonstrate below, unconverged or poorly converged states may mislead us in understanding the spectrum.

Large  $K$  implies large  $k$  for given  $R$  and  $\tau$ , and hence our calculation demands bigger dimensionality  $N$  of the truncated Hilbert space, since the PR is roughly increasing as  $k^2$ . Although we take  $N = 2000$ , getting a good number of converged states is problematic. We pursue the spacing distribution with different convergence criteria for the numerically obtained states. The convergence criteria uses partial sum of the state components :

$$\{\text{Sum}\}_M = \sum_{n=1}^M |\psi_n|^2 \quad ; \quad \text{with } M < N. \quad (27)$$

For a well converged state we expect that  $\{\text{Sum}\}_M \approx 1$ , even for  $M \ll N$ . We denote by  $N_M$  the number of converged eigenstates whose  $\{\text{Sum}\}_M$  is greater than  $S_M$  (an arbitrary number close to, but less than, unity) for a fixed value of  $M$ . Thus the convergence criteria is characterized by  $M$  and  $S_M$ .

In Fig. 12, we have shown the spacing distributions with different criteria for two cases. In both the cases transition to Wigner distribution is evident as the convergence criteria is relaxed. The unconverged or poorly converged states do not belong to the physical system of our interest and the corresponding quasienergies follow the RMT prediction. Obviously, reliability of the result is more in the top plots where the spacing shows neither Poisson nor Wigner distributions. Though the tail part shows the Poisson behaviour there are significant discrepancies in the small spacing. A more correct picture may be closer to the scenario of the chaotic regimes presented in Fig. 10.

Shown in Fig. 13 are few “well converged” states, with more stringent convergence criteria ( $M = 1600, S_M = 0.9999$ ). With this criteria we have only  $N_M = 12$  and 4 for  $R = 1$  and 0.5 respectively. The state components exhibit strong fluctuations in the basis. Here again it is hard to differentiate the two cases qualitatively. The states corresponding to  $R = 0.5$  also appear to have exponential tails. To see the distribution of the state components, we introduce a variable  $\eta_n = |\psi_n|^2 / \overline{|\psi_n|^2}$  where over bar stands for average over the state components such that  $\overline{\eta} = 1$ . As seen from Fig. 14, the cumulative distribution of  $\eta$  for both the cases have very similar behaviour. Considerable deviations from the RMT predicted cumulative Porter-Thomas distribution,  $I(\eta) = \text{Erf}(\sqrt{\eta/2})$ , may be attributed to the localization of the states. However, the distribution corresponds to  $R = 0.5$  tends to be closer to the RMT predicted behaviour.

## V. SUMMARY AND CONCLUSION

A particle inside a one-dimensional infinite square well potential in the presence of a time periodic pulsed field is examined both classically and quantum mechanically. This simple model can be seen as one generalization of the kicked rotor, or the standard map. A variety of classical dynamical features emerge from the nature of the ratio,  $R$ , of the two competing length scales (the well width and field wavelength). Many of the dynamical features so observed are generic to a wide class of systems of substantial current interest *viz.* externally forced particles in wells.

It is shown that when the length scales do not match, even in perturbative regimes dynamics can be increasingly complex wherein all the KAM tori in phase space break up. As a result the transition to chaos is abrupt, a typical scenario of non-KAM behaviour. Quantum

mechanically imprints of such a transition is seen as a spread in bulk part (delocalization) of the eigenstates. Thus we realize the length scale ratio  $R$  as a control parameter for the localization in the weak field regime.

On increasing the field strength, chaos assisted diffusion takes place in momentum. From earlier studies on the kicked rotor it is known that the average localization length of the eigenstates is directly proportional to the classical diffusion coefficient. We have shown that in our generalization of the kicked rotor also, this result grossly explains the localization behaviour of the eigenstates through the classical transport property. Thus the kicked rotor continues to serve as a useful model in understanding physical phenomena exhibited by a larger class of systems.

We have observed, as expected, that in the regular case the nearest neighbour spacing distribution of the quasienergies show good agreement with Poisson distribution. We have presented evidence to support that, in highly chaotic regimes spacings show some deviations from the Poisson distribution though the corresponding eigenstates belong to an unbounded phase space. Limited overlap of the eigenstates results in such deviations. However, spacing does not show the RMT predicted Wigner distribution as was claimed in an earlier study [17]. The earlier result is attributed to lack of converged states which make up the statistics.

While spacing is not much sensitive to the classical chaos, the distribution of participation ratios of the eigenstates is shown to be a good measure to distinguish chaotic quantum systems from the regular ones. Quantum mechanically, chaotic regimes are characterized by a lognormal distribution of the participation ratios. In addition to the above generic quantum features, we have also studied non-generic phenomena like “quantum resonance”. In resonance condition, kinetic energy of the particle grows quadratically with the number of kicks. This unbounded energy growth is not affected by the length scale ratio and can enhance ionization in the finite well system.

As far as experimental realizations of this work is concerned, perhaps both quantum wells [3] and cold atom experiments [15] are possible candidates. As suggested above, the  $R$  effects may be best observed at small field strengths and for  $R > 1$ . Further work is underway exploring the nature of localization in such systems, including a bounded version of the generalized standard map.

## REFERENCES

- [1] F. Haake, *Quantum Signatures of Chaos*, Springer-Verlag (1991).
- [2] H-J. Stockmann, *Quantum Chaos : an introduction*, Cambridge Univ. Press (1999).
- [3] P.B. Wilkinson, T.M. Fromhold, L. Eaves, F.W. Sheard, N, Miura and T. Takamasu, Nature bf 380, 608 (1996).
- [4] L.E. Reichl, *The Transition to Chaos*, Srpinger-Verlag, New York (1992).
- [5] M.V. Berry, N.L. Balazs, M. Tabor and A. Voros, Ann. Phys. **122**, 26 (1979).
- [6] G. Casati, B.V. Chirikov, J. Ford and F.M. Izrailev, *Lecture Notes in Physics* Vol.93, 334 (1979).
- [7] B.V. Chirikov, Phys. Rep. **52**, 263 (1979); B.V. Chirikov, *Review of Plasma Physics* Vol.13, 1 (1987).
- [8] J.M. Greene, J. Math. Phys. **20**, 1183 (1979).
- [9] S.J. Shenker and L.P. Kadanoff, J. Stat. Phys. **27** (4), 795 (1982).
- [10] A.J. Lichtenberg and M.A. Lieberman, *Regular and Chaotic Dynamics*, Springer-Verlag, (1992).
- [11] F.M. Izrailev, Phy. Rep. **196**, 299 (1990).
- [12] A. Lakshminarayan, N.R. Cerruti and S. Tomsovic, Phys. Rev. E, **60**, 3992 (1999); Phys. Rev. E, **63**, 016209-1 (2000).
- [13] D.R. Grempel, R.E. Prange and Shmuel Fishman, Phys. Rev. A, **29**, 1639 (1984).
- [14] P.W. Anderson, Phys. Rev. **109**, 1492 (1958).
- [15] F.L. Moore, J.C. Robinson, C.F. Bharucha, Bala Sundaram and M.G. Raizen, Phys. Rev. Lett. **75**, 4598 (1995); J. Ringot, P. Szriftgiser, J.C. Garreau and D. Delande, Phys. Rev. Lett. **85**, 2741 (2000).
- [16] T.A. Brody, J. Flores, J.B. French, P.A. Mello, A. Pandey, and S.S.M. Wong, Rev. Mod. Phys. **53**, 385 (1981).
- [17] Bambi Hu, Baowen Li, Jie Liu and Yan Gu, Phys. Rev. Lett. **82**, 4224 (1999).
- [18] R. Sankaranarayanan, A. Lakshminarayan, and V.B. Sheorey, Phys. Lett. A **279**, 313 (2001).
- [19] Ya.B. Zel'dovich, Soviet Physics JETP, **24**, 1006 (1967).
- [20] F.M. Izrailev and D.L. Shepelyanskii, Theor. Math. Phys. **43**, 553 (1980).
- [21] B.V. Chirikov, F.M. Izrailev and D.L. Shepelyansky, Sov. Sci. Rev. **2C**, 209 (1981).
- [22] D.L. Shepelyansky, Phys. Rev. Letts. **56**, 677 (1986); Physica D **28**, 103 (1987).
- [23] J. Aitchison and JAC Brown, *Lognormal Distribution : With special reference to its uses in Economics*, Cambridge Univ. Press (1957).
- [24] O.A. Starykh, P.R.J. Jacquod, E. Narimanov and A.D. Stone, Phys. Rev. E **62**, 2078 (2000).

FIGURES

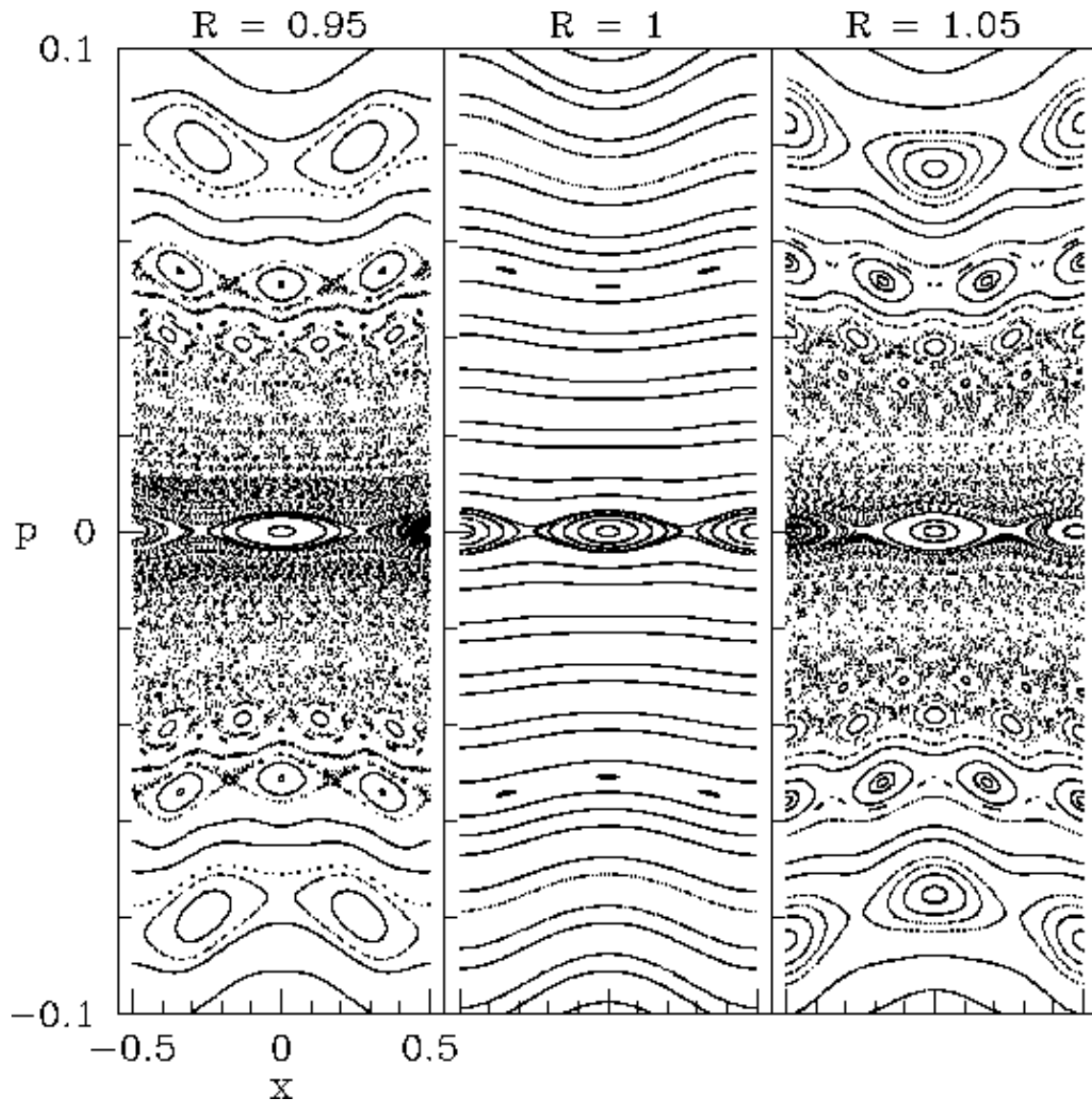


FIG. 1. Typical phase space of the system governed by the Hamiltonian in (1) with  $\epsilon = 0.001$  and  $\omega = 1$ . The lower momentum region is increasingly chaotic when the length scales do not match.



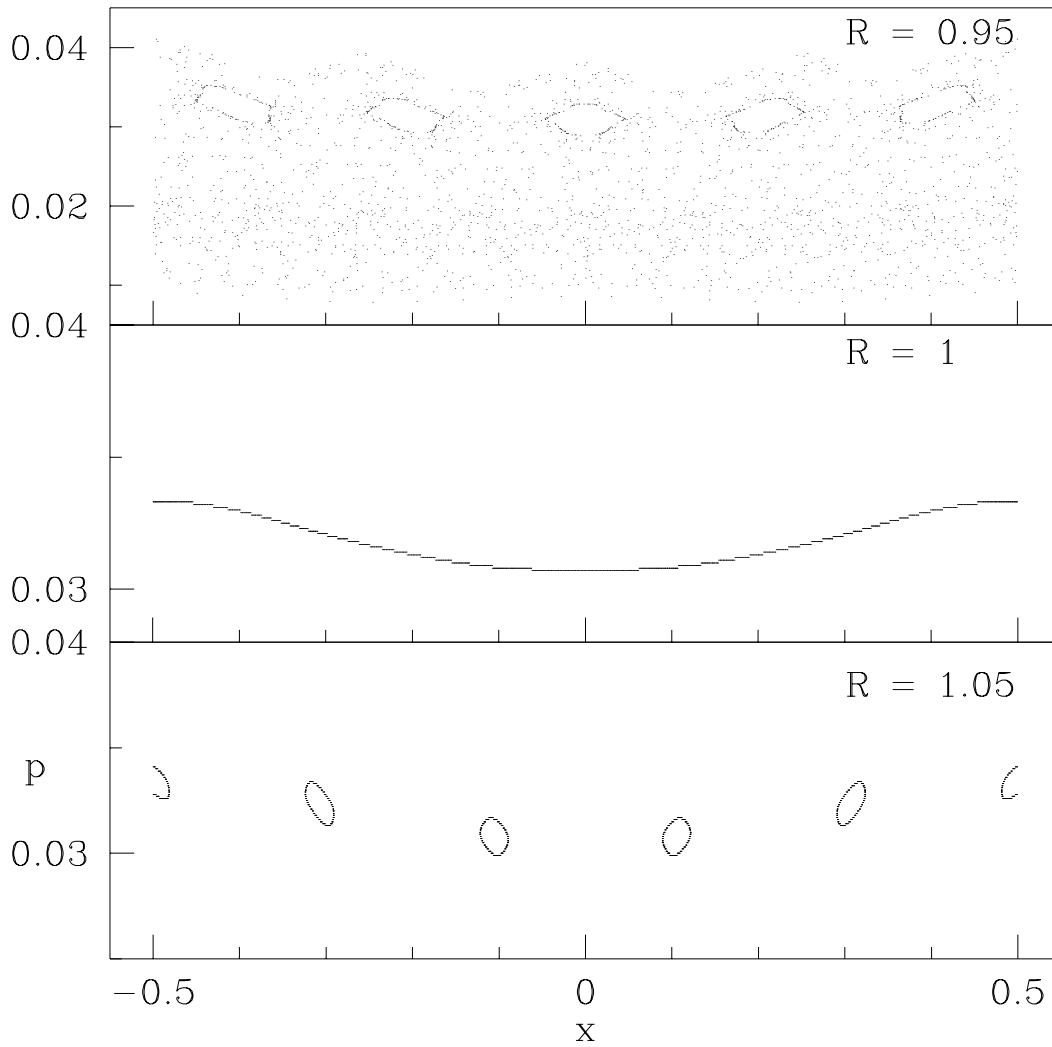


FIG. 2. Shown are orbits of Fig. 1 having identical initial conditions. The initial condition corresponds to a KAM torus in the lower momentum region for  $R = 1$  (the negative momentum region is not shown here). Note the abrupt change in the stability and the non-generic features of the resultant phase space structures.

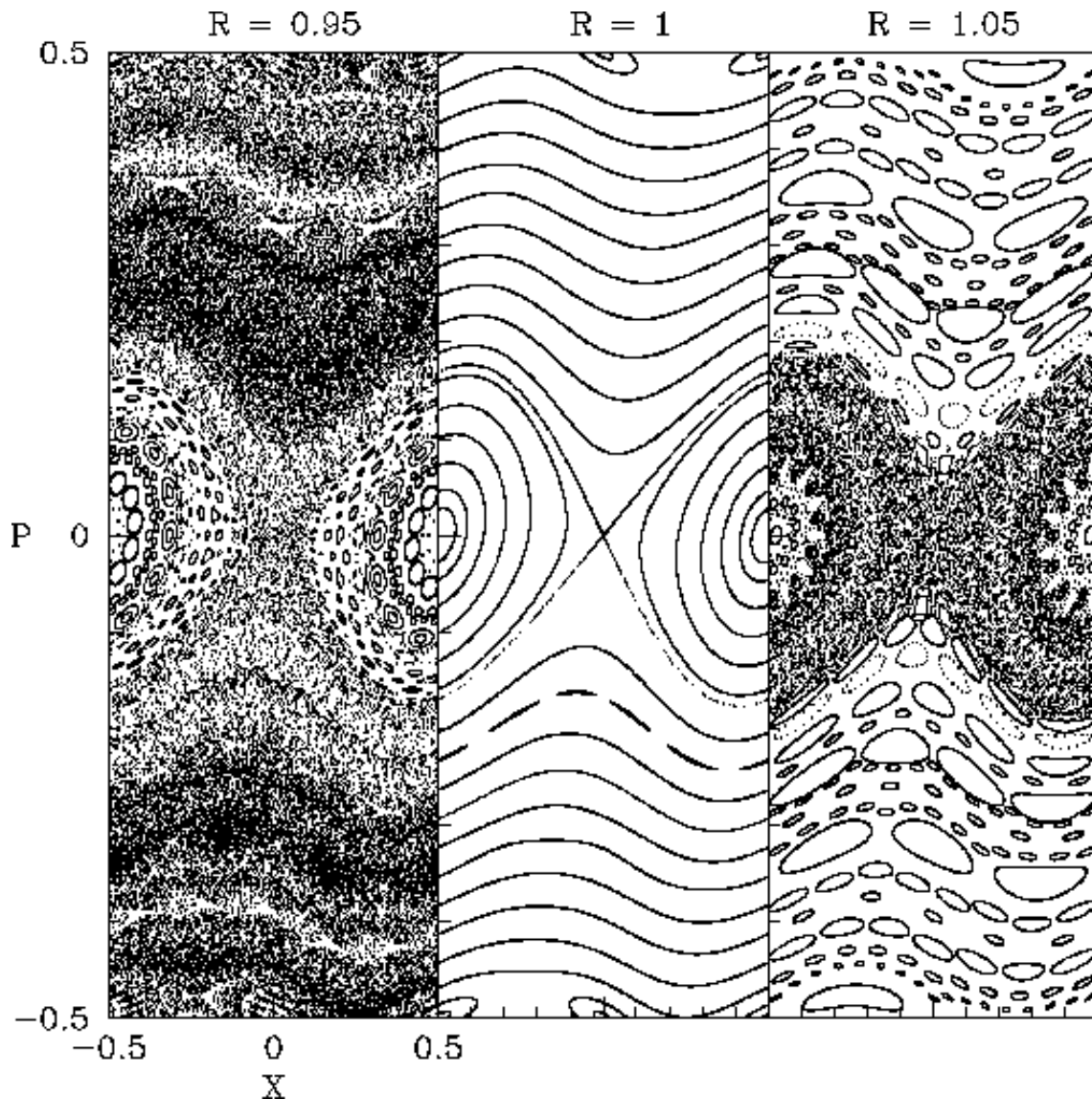


FIG. 3. Phase space portrait of the GSM with  $K = 0.3$ . For  $R = 1$ , the dynamics is nearly regular wherein many smooth KAM tori are seen. When  $R$  departs from unity the dynamics is increasingly complex and no KAM tori are seen. This may be compared to the lower momentum region in Fig. 1.

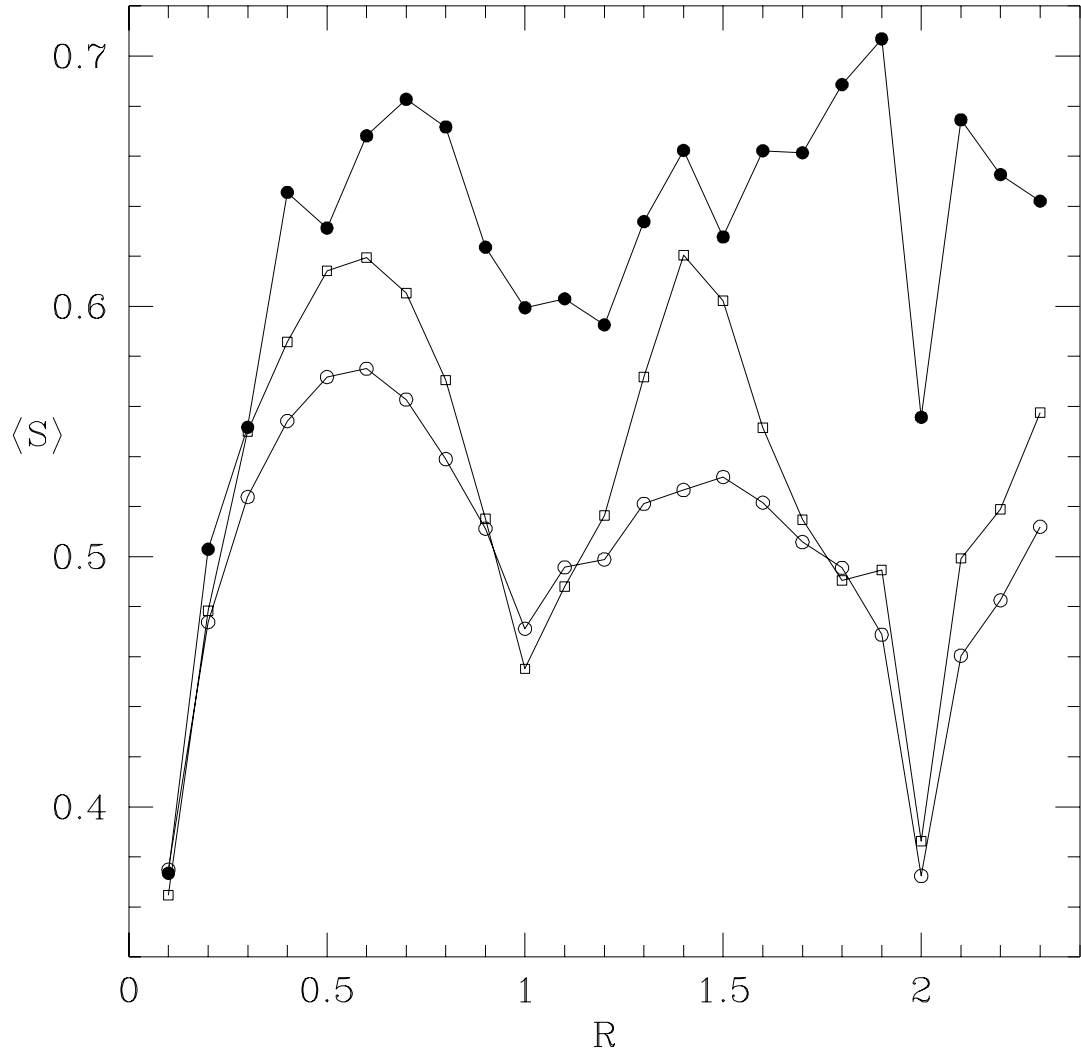


FIG. 4. Average entropy of 1000 eigenstates for :  $K = 0.1, \tau = 0.001$  ( $\circ$ );  $K = 1, \tau = 0.01$  ( $\square$ );  $K = 10, \tau = 0.1$  ( $\bullet$ ).  $N = 1200$  in all the cases.

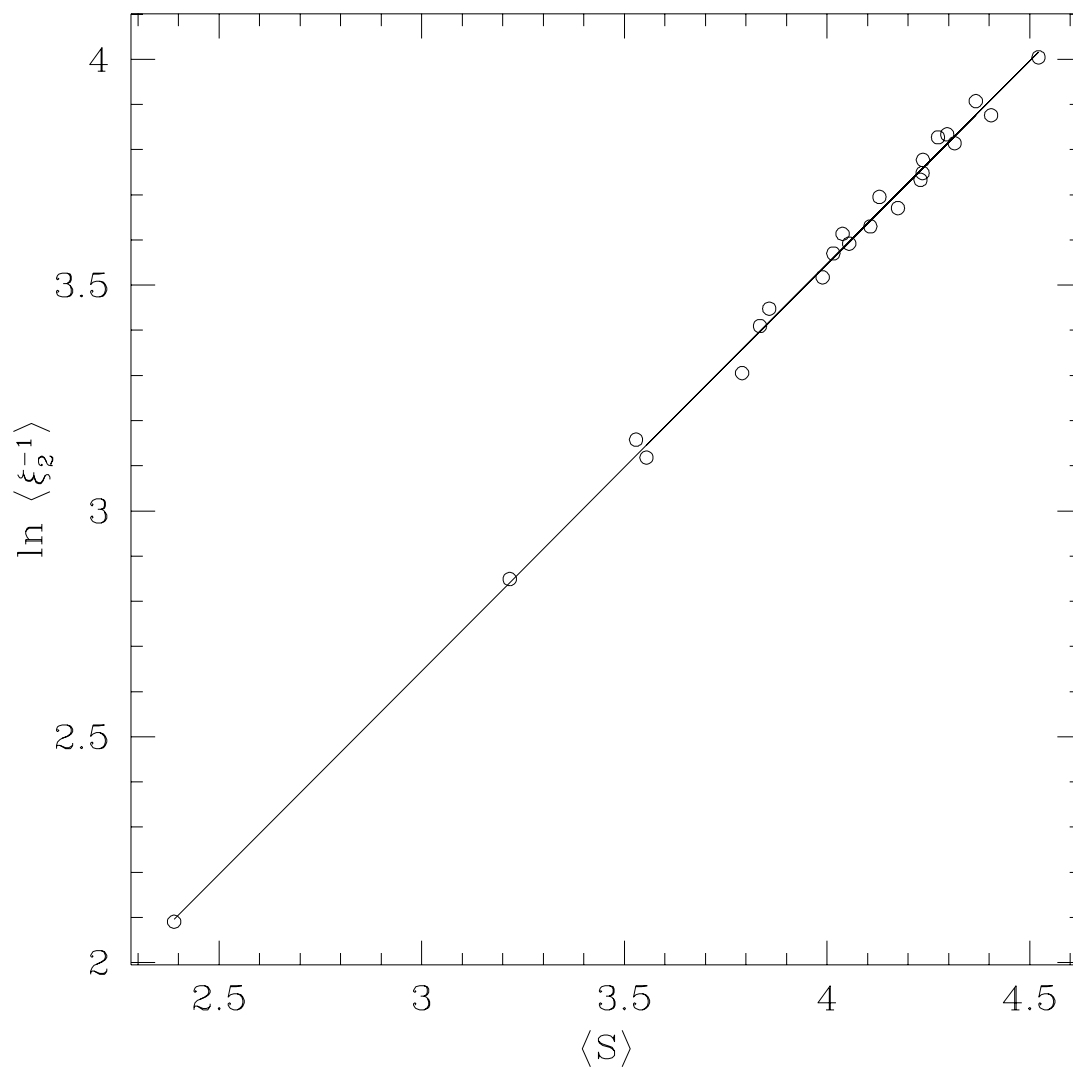


FIG. 5. Average entropy .vs. the log of the average PR corresponding to the case  $K = 10, \tau = 0.1$  of Fig. 4. The slope of the fitted straight line is  $0.9 \pm 0.01$ .

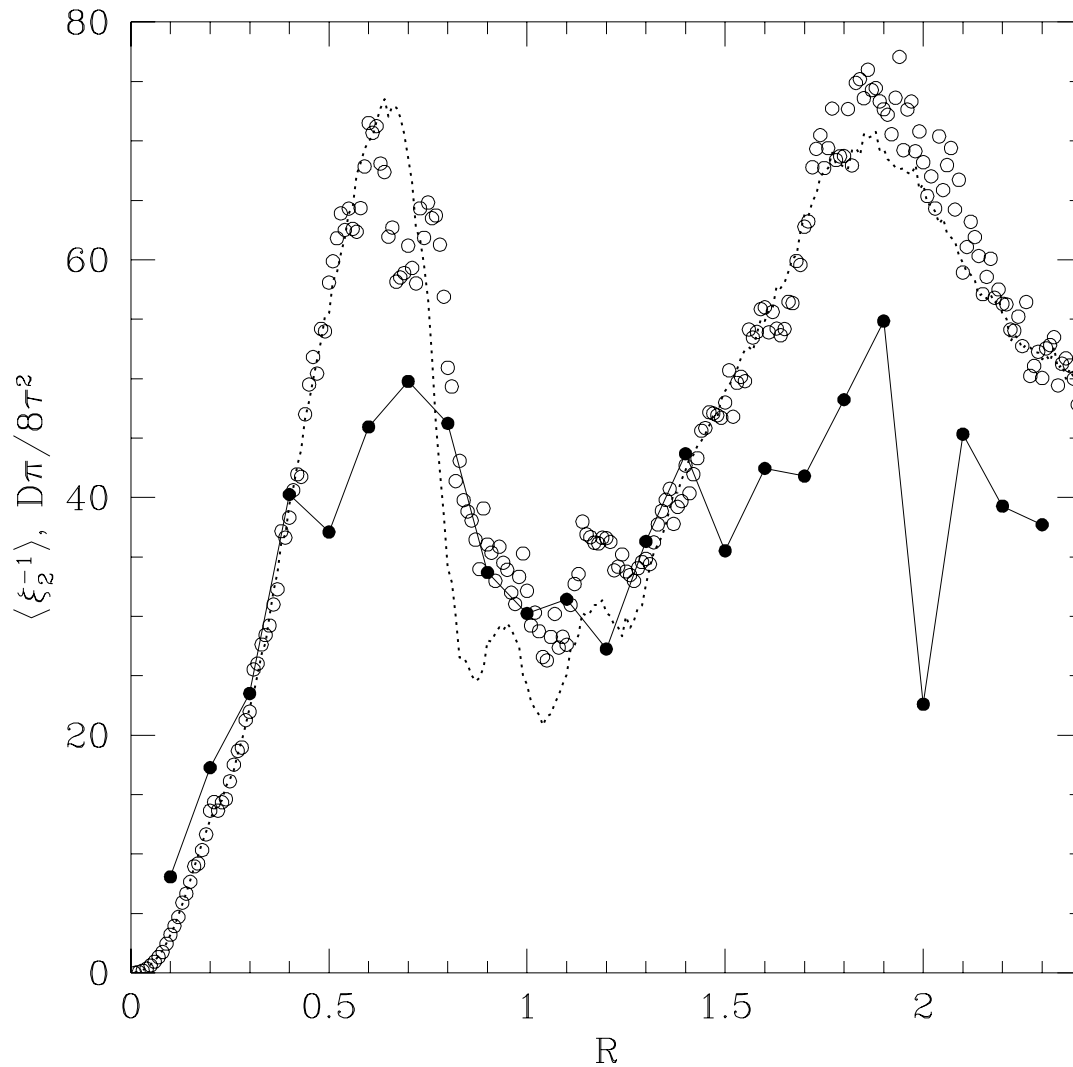


FIG. 6. The average PR ( $\bullet$ ) and the scaled classical diffusion coefficient ( $\circ$ ) are plotted as a function of  $R$  for the case  $K = 10, \tau = 0.1$ . The dotted line is the scaled coefficient calculated using up to the second order time correlation. Higher order time correlations are insignificant since the classical system is highly chaotic.

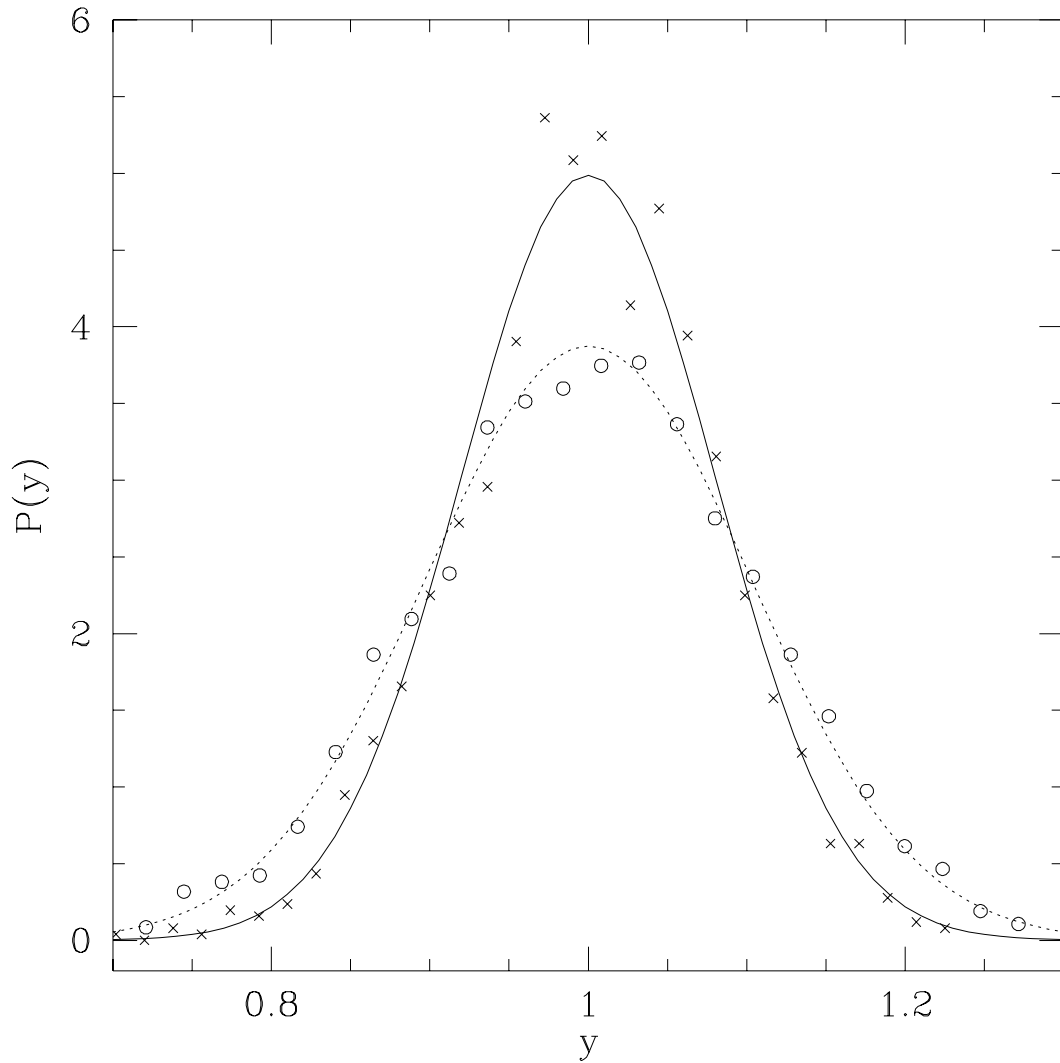


FIG. 7. Probability distribution of  $y$ , the normalized log of the PR, for the kicked rotor case ( $R = 1$ ) in the chaotic regime. Here we have taken  $K = 10$  and  $\tau = 0.025$  ( $\times$ ),  $\tau = 0.05$  ( $\circ$ ). Smooth curves are corresponding gaussian distributions.

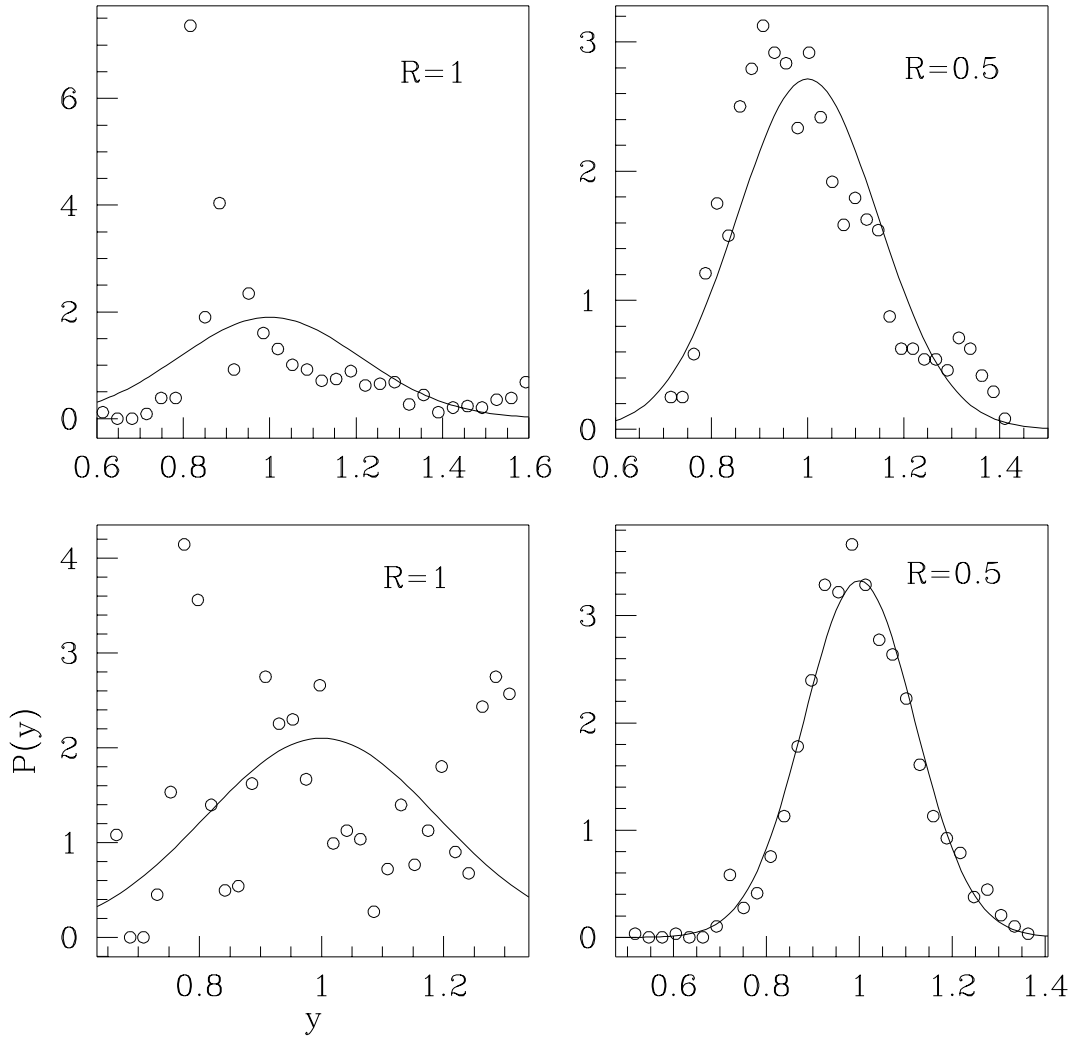


FIG. 8. Probability distribution of  $y$ , the normalized log of the PR, for the case  $K = 0.1, \tau = 0.001$  (first row) and for  $K = 1, \tau = 0.01$  (second row). Smooth curves are corresponding gaussian distributions. Note the sensitivity of these distributions to the classical dynamics.

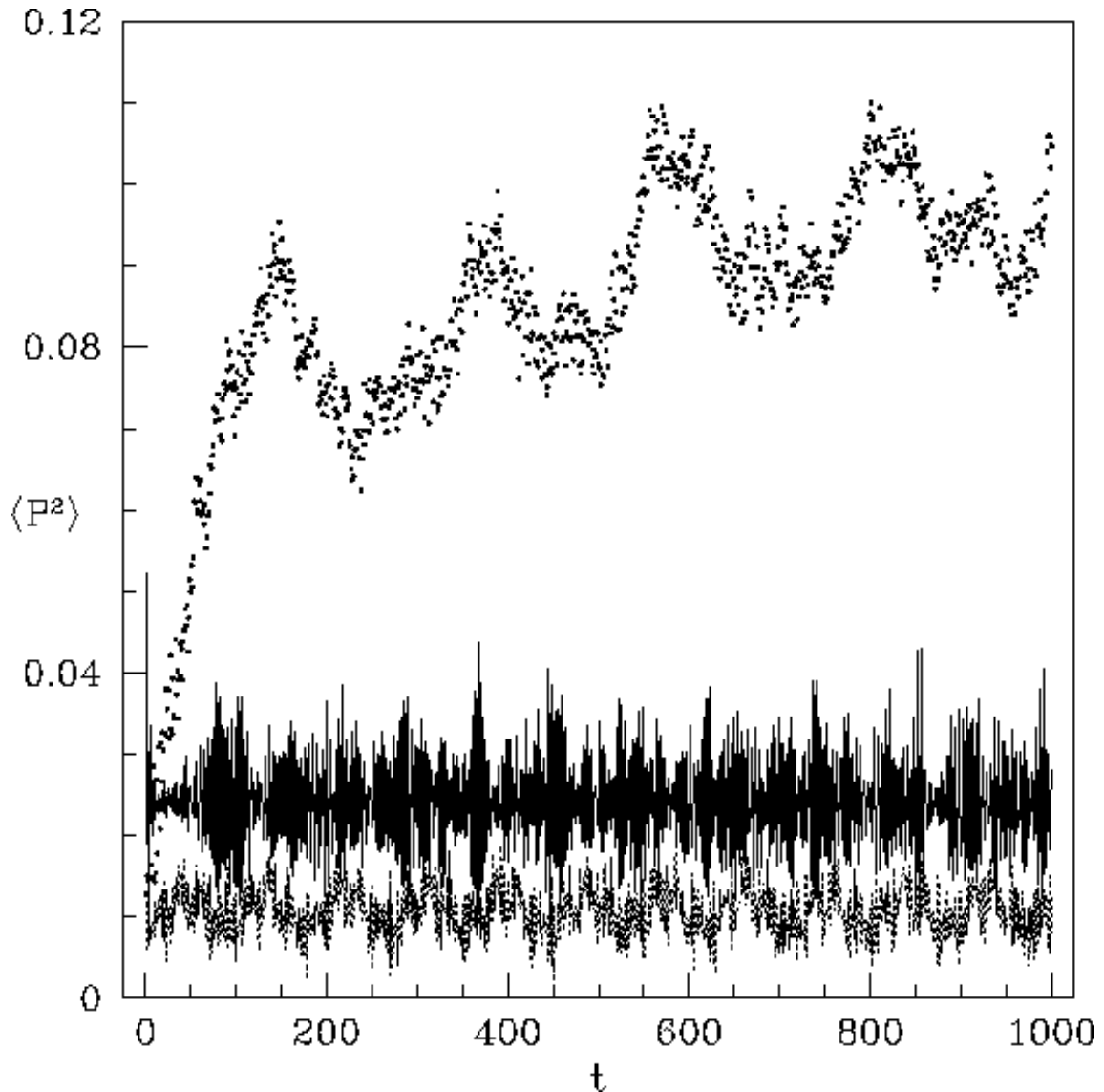


FIG. 9. Shown is the scaled kinetic energy  $\langle P^2 \rangle$  of a state, which is initially the ground state of the unperturbed system, as a function of time. Here the parameters are  $K = 1, \tau = 0.01$ ;  $R = 1$  (solid line),  $R = 1.5$  (dots) and  $R = 2$  (dotted line). Effect of non-integer  $R$  is remarkably seen in the evolution as the kinetic energy of the quantum particle saturates at much higher value compared to integer  $R$  cases.



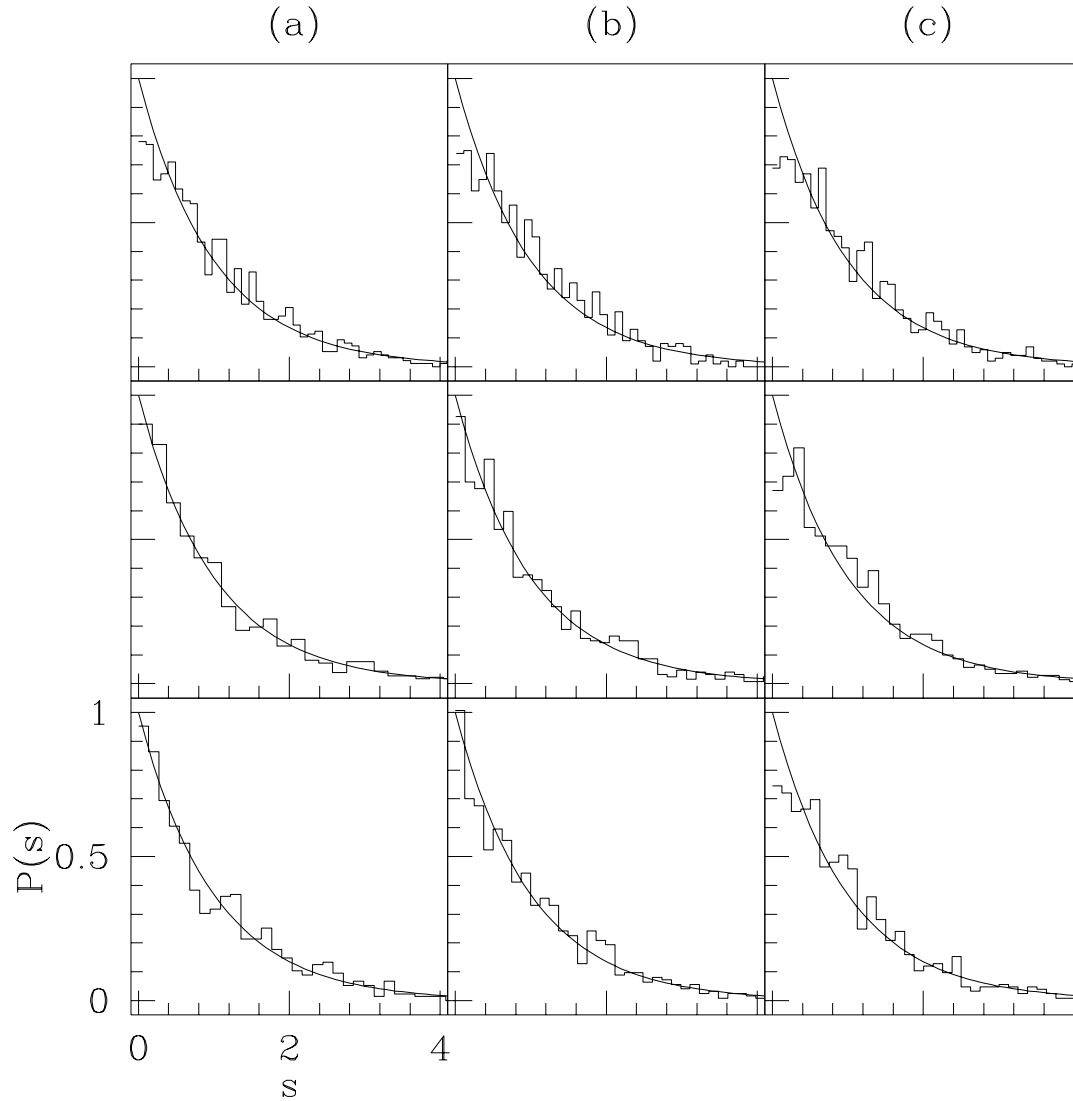


FIG. 10. Nearest neighbour spacing distributions of 1000 quasienergies for (a)  $K = 0.1, \tau = 0.001$ ; (b)  $K = 1, \tau = 0.01$ ; (c)  $K = 10, \tau = 0.1$  with  $R = 0.5, 1, 1.5$  (top to bottom) and  $N = 1200$ . Smooth curves are Poisson distributions. Note the relative insensitivity of these distributions to the classical dynamics.

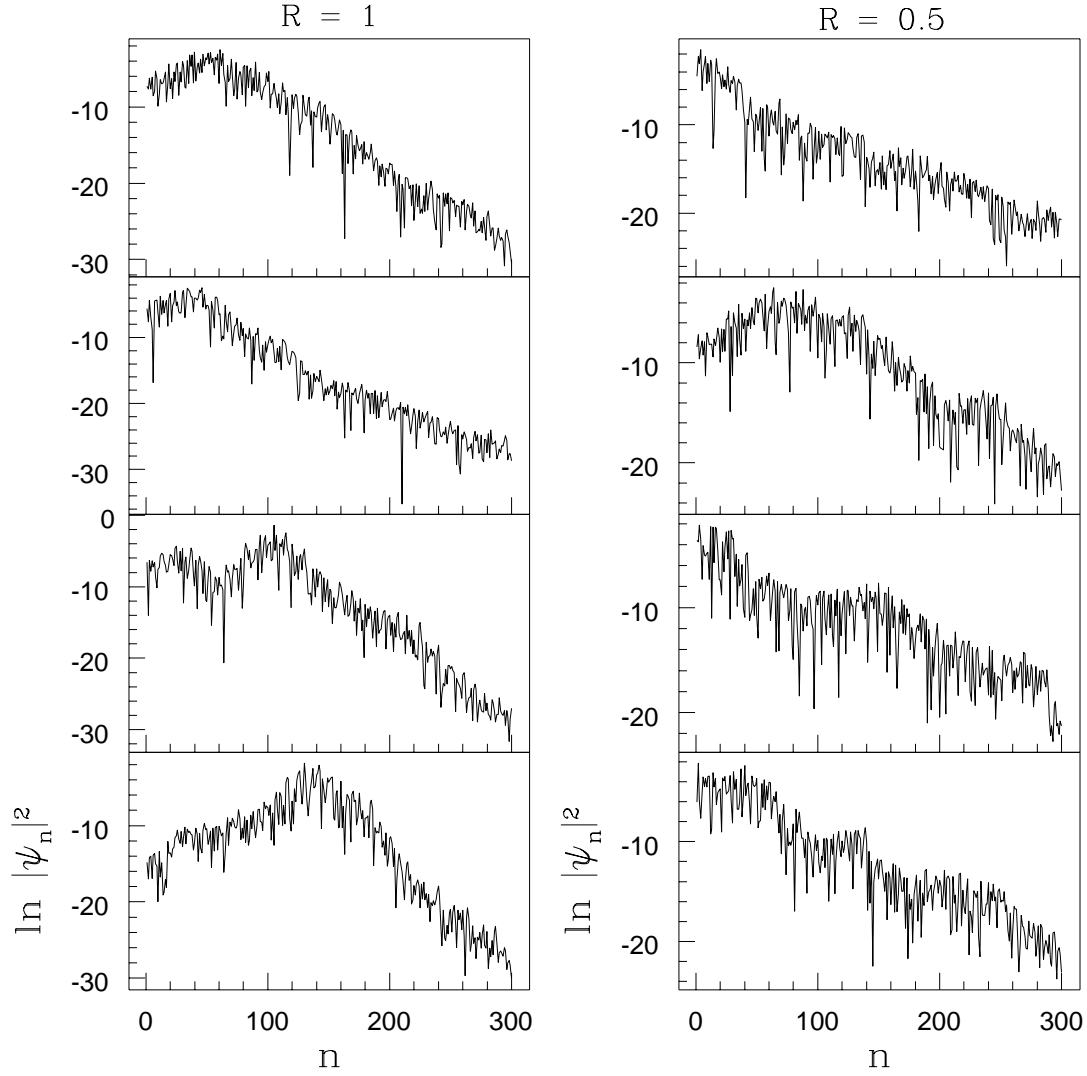


FIG. 11. Typical eigenstates for the case  $K = 10, \tau = 0.1$ . States corresponding to  $R = 0.5$  have more fluctuations compared to the rotor ( $R = 1$ ) states.

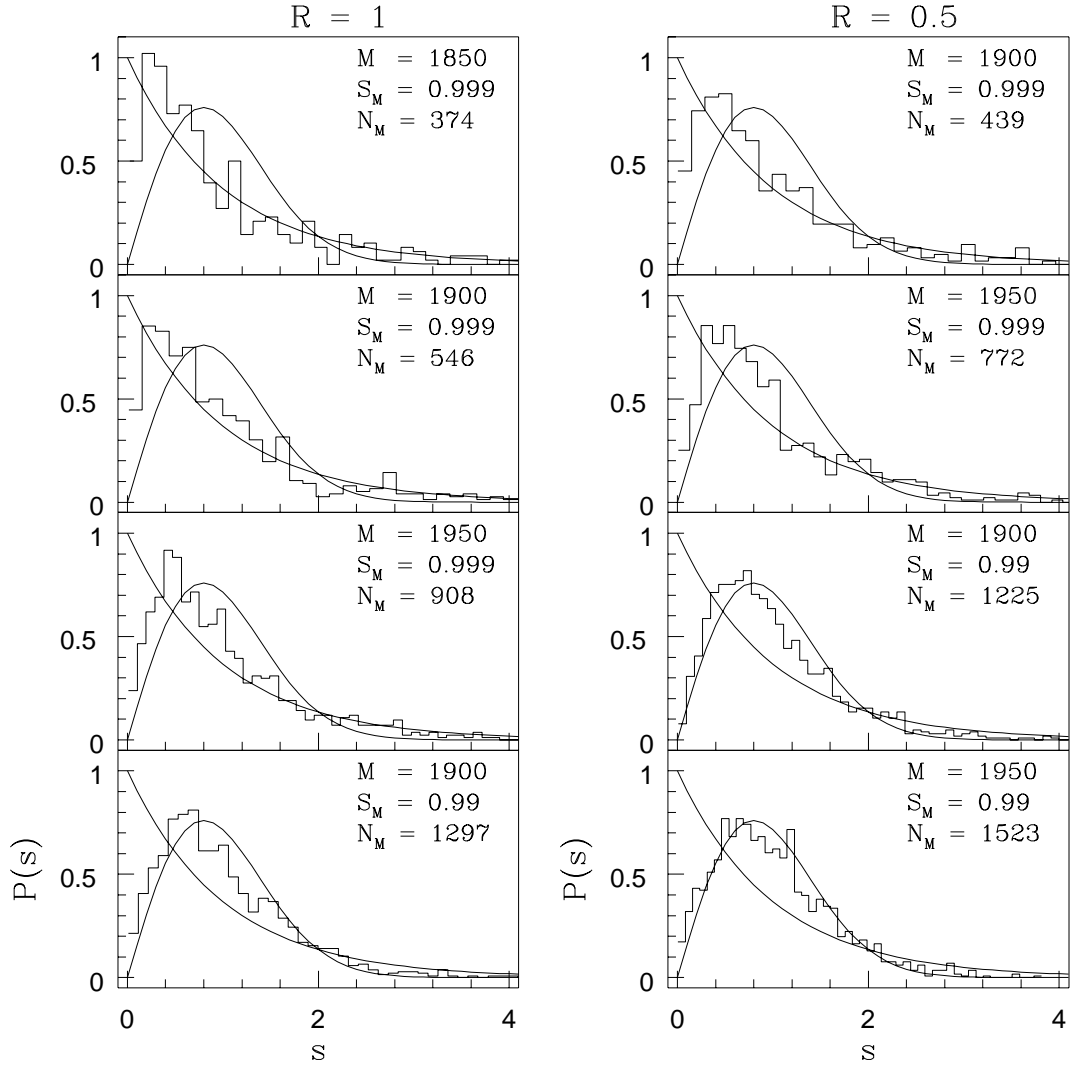


FIG. 12. The nearest neighbour spacing distributions for the case  $K = 50, \tau = 0.1$ . Smooth curves are the Poisson and Wigner distributions. Convergence criteria is relaxed as we move from top to bottom. A “spectral transition” is observed.

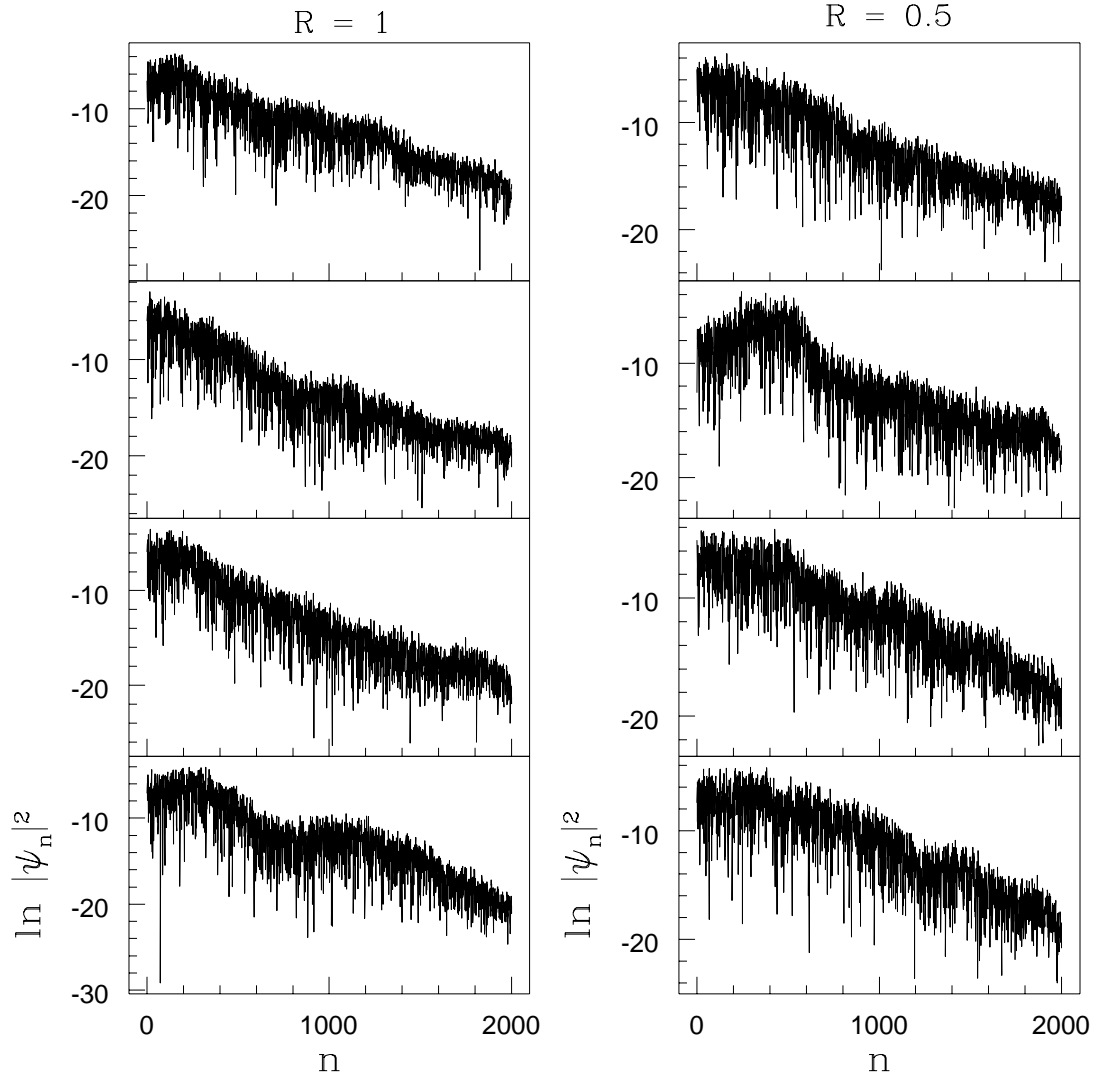


FIG. 13. Typical well converged eigenstates for the highly chaotic case:  $K = 50, \tau = 0.1$  and  $N = 2000$ .

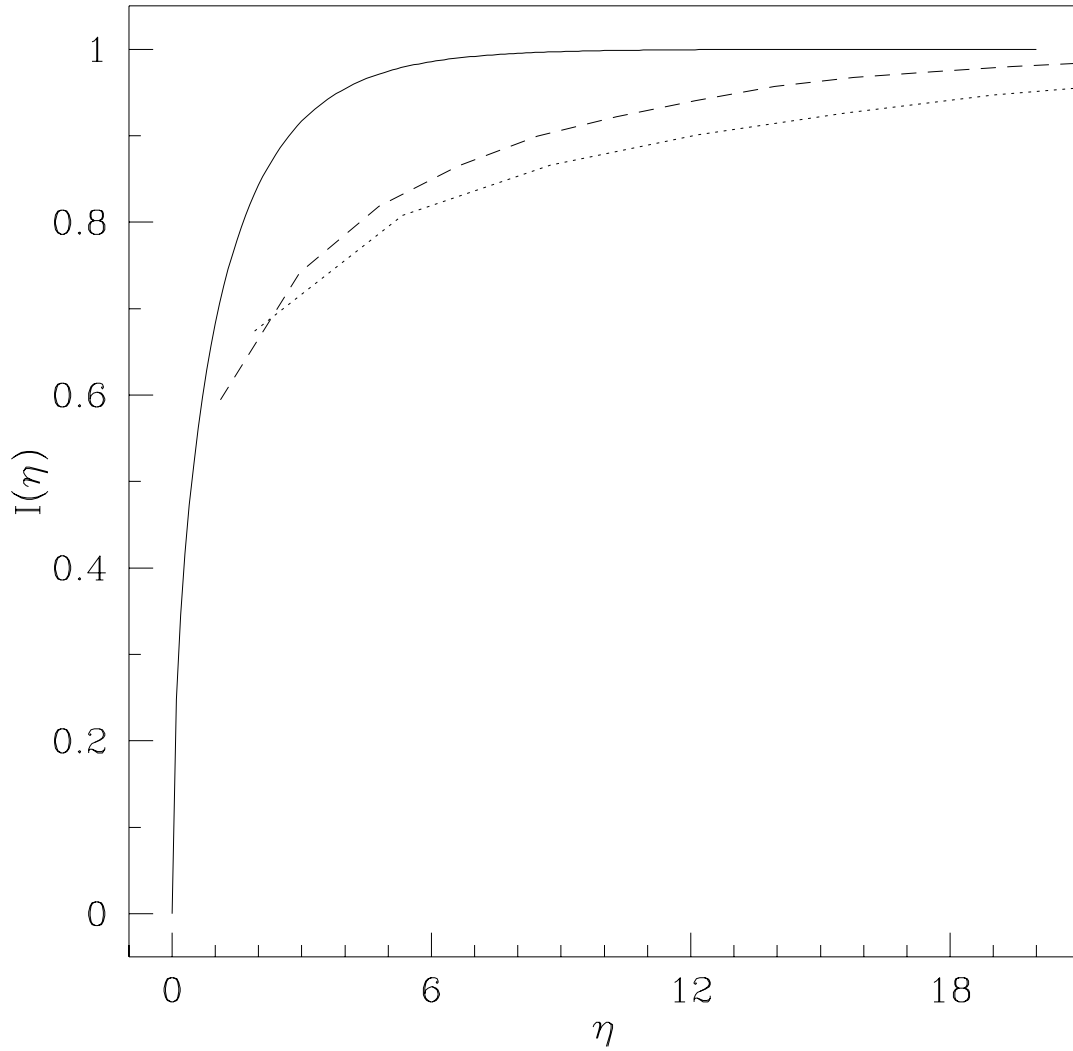


FIG. 14. Collective cumulative distribution of the components of the states shown in Fig. 13. Dotted curve corresponds to  $R = 1$  while dashed curve corresponds to  $R = 0.5$ . Solid curve is the cumulative Porter-Thomas distribution.